Acta Polytechnica CTU Proceedings **50**:30–35, 2024
https://doi.org/10.14311/APP.2024.50.0030

Published by the Czech Technical University in Prague

NANOMECHANICAL PROPERTIES OF NEUTRON-IRRADIATED CONCRETE

Ondřej Libera[a], Jiří Němeček [1,b], Patricie Halodová[a,*], Zbyněk Hlaváč[a], Jiří Němeček [2,b]

[a] *Research Centre Řež, Department of Material and Mechanical Properties, Hlavní 130, 250 68 Husinec-Řež, Czech Republic*

[b] *Czech Technical University in Prague, Faculty of Civil Engineering, Department of Mechanics, Thákurova 7, 166 29 Prague 6, Czech Republic*

[*] corresponding author: patricie.halodova@cvrez.cz

Abstract. Concrete exposed to irradiation from nuclear reactor undergoes atomic-level degradation due to the influence of neutrons, secondary gamma rays, and associated gamma heating. The radiation-induced damage decreases the mechanical properties of the concrete and affects its performance as a construction material. The concrete samples analysed in this work were prepared from blended Portland cement CEM II 32.5R mixed with siliceous aggregates with a size of 0–2.5 mm. The material underwent irradiation in the LVR-15 research reactor in Research Centre Řež to the target neutron fluence of $1.6–1.8 \cdot 10^{19}$ n cm^{-2} (E>0.1 MeV) and received the gamma dose of ∼500 MGy. The temperatures during irradiation were kept within a range of 50–60 °C. The mechanical properties of the individual phases in the cementitious matrix after neutron irradiation were assessed by the nanoindentation. To track the evolution of the nanomechanical properties of individual components under radiation, a comparison was made between the mechanical properties of neutron-irradiated material and pristine concrete.

Keywords: Concrete, nanoindentation, neutron irradiation, mechanical properties.

1. Introduction

With increasing demands for power generation and nuclear safety all materials used in nuclear reactor are a subject of precise examination regarding degradation caused by long-term radiation exposure [1, 2]. Concrete is an essential construction material for various types of nuclear reactor power plants, providing the structural foundation for the reactor pressure vessel and serving as a component of radiation shielding. The irradiation effects influence the behaviour of the concrete structure, leading over time to alterations in its mechanical properties and potential failure [3, 4]. The material degradation caused by gamma and neutron radiation significantly impacts the functional and performance requirements of the shield [5]. Micro-scale analyses of the concrete material are needed to observe the actual changes in the material via irradiation. In this work, microscopic analyses are combined with micromechanical testing to evaluate the effects of neutron irradiation on the microstructure of the concrete. Specifically, cement paste of the concrete and its major phases are a matter of examination. The mechanical properties of the cement paste are measured by nanoindentation testing. Typically, this can be done by a matrix array of indents over the large area with subsequent statistical deconvolution of the data [5–7]. However, this method may be inadequate for distinguishing the mechanical properties of irradiated materials from those of the reference equivalent. This limitation arises due to the overlapping measured values of the individual phases present in the cement paste, as the anticipated changes in mechanical properties after the irradiation are within the range of a few percent. Therefore, we propose an alternative approach in which nanoindentation measurements are manually positioned, and the indented phases are identified using optical microscopy and scanning electron microscopy (SEM) coupled with energy dispersive x-ray spectroscopy (EDS). The resulting data from measurements of individual phases could serve as a key to interpreting extensive datasets obtained from wide area matrix measurements.

2. Materials and methods

2.1. Concrete

The concrete samples were manufactured using the standard procedure following ČSN EN 206-1 [8]. The used binder component was blended Portland cement CEM II 32.5R (Portland cement 62 %, limestone 11 %, fly ash 21 %, gypsum 6 % by mass) mixed with siliceous aggregates with a grain size of 0–2.5 mm used as a filler. The samples were left for 28 days in closed containers for curing and hardening, subsequently stored for 18 months in laboratory conditions with $T = 23 \pm 1$ °C, RH 45 ± 5 % and afterwards cut into slices with ap-

[1] Postdoctoral researcher at Czech Technical University in Prague, ORCID: 0000-0002-5635-695X.

[2] Professor at Czech Technical University in Prague, ORCID: 0000-0002-3565-8182.

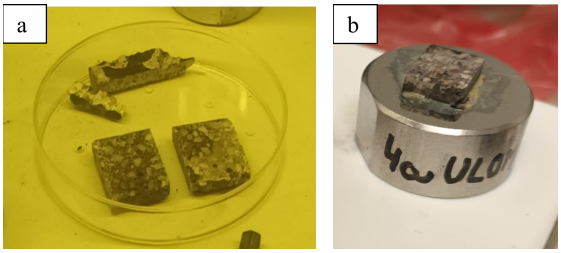

(A). (B).

FIGURE 1. Cut neutron irradiated concrete slices (A). Mounted concrete sample on a steel block (B).

prox. size of $28 \times 28 \times 5$ mm, dried at 60 % for 7 days and then placed in the irradiation channel and assembly designed and developed for long-term irradiation campaign in LVR-15 research reactor. The irradiation was carried out in 6 campaigns over a period of 170 days [9]. The reference cement sample was produced using the original recipe, the composition of Portland cement CEM II 32.5R slightly differed (Portland cement 76 %, limestone 18 %, gypsum 6 % by mass).

2.2. Neutron irradiation

Neutron irradiation was performed in the LVR-15 research reactor with a power of 10 MW in Research Centre Řež to the target neutron fluence of $1.6–1.8 \cdot 10^{19}$ n cm^{-2} (E>0.1 MeV) with the received gamma dose of $\sim$ 500 MGy. The temperatures during irradiation were kept within a range of 50–60 °C. Such fast neutron fluences correspond approximately to 40 years of operation of the biological shielding components at the Dukovany Nuclear Power Plant (NPP-EDU) of VVER-440 type. This allows for the simulation of concrete degradation due to neutron flux corresponding to the entire planned lifespan of the NPP. After the irradiation, the housing with samples were transported to hot-cells, where cutting, dismounting, and sorting was performed using remote manipulators. Samples intended for nanoindentation were transferred to shielded glove-box for further surface preparation.

2.3. Sample preparation

After the neutron irradiation, the concrete samples were cut in gamma-shielded glove box into smaller pieces in cross-section using gravitational low-speed saw (Buehler). The dimensions of cut sample were approx. $1.5 \times 1.3 \times 0.5$ cm. The reduction of sample dimensions was necessary for the surface preparation process and for the overall reduction of radioactivity of the sample. Cut concrete samples are shown in Figure 1a.

After the cutting, the irradiated concrete sample was glued to cylindrical steel block using hot wax (Figure 1b). Mounting of the sample was performed for easier manipulation during the hand-polishing process

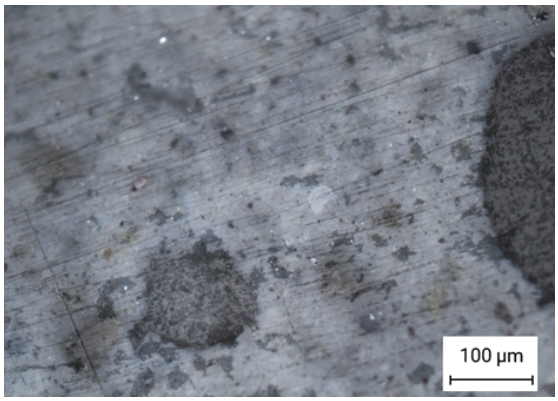

FIGURE 2. Light optical microscopy image of cement phase after grinding.

and for better handling during nanoindentation and SEM analyses.

Surface preparation of the neutron irradiated concrete sample was performed by dry hand grinding using silicon carbide sandpapers of 400–4 000 grit in gamma-shielded glove box. No water was used during the grinding process to prevent further hydration of the cement paste and to achieve uniform flat surface. Adding water during the grinding process would cause higher erosion in the cement paste and therefore uneven surface. For those two reasons, further polishing using suspensions was not used. The surface of the ground irradiated concrete sample was washed with pure ethanol after each grinding step. The whole surface preparation process was identically performed for the reference non-irradiated concrete sample.

Quality of prepared surface was assessed by light optical microscopy. The cement paste area of interest (light) is shown in Figure 2. Larger dark areas in the image are siliceous aggregates that are not a subject of examination in this work. The surface in Figure 2 has uniform flatness and good visibility of features in the cement paste. Visible scratches on the surface are an unavoidable phenomenon due to the applied surface preparation method. However, the unscratched areas between the scratches can be hand selected for nanoindentation measurements in nanoindenter scanning probe microscopy (SPM) mode.

A 20 nm conductive carbon layer was deposited on the ground surface prior to SEM measurements with PVD carbon coater.

2.4. Nanoindentation

Nanoindentation measurements were performed in gamma-shielded hot cell with Bruker Ti 950 nanoindenter using Berkovich diamond indenter tip at room temperature. Positions for the measurements were hand selected on the SPM scan of the surface performed by the nanoindenter tip. Individual selected positions are shown in Figure 3. The dimensions of the SPM scan area were 70×70 µm.

Load-controlled indentation mode with 4 mN max. indentation force was selected for nanoindentation

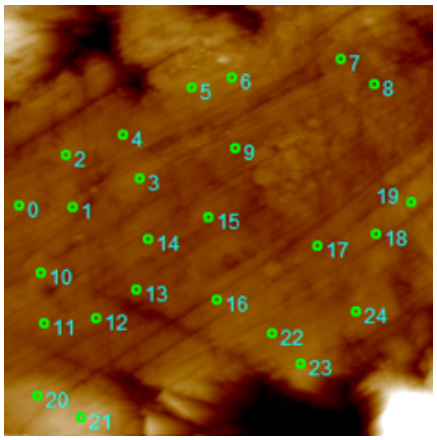

Figure 3. Hand selected indent positions on the SPM scan image of the cement paste.

measurements. The estimated size of indented area using this load in cement paste is approx. 3 µm in diameter with indentation depth in the range of 300–500 nm. A custom load function with three stages was used: 1 s linear load, 10 s hold, 1 s linear unload. The hold period was used for material relaxation under load and for possible short-term creep behaviour. Measured load-displacement curves were analysed by the Oliver-Pharr method [10]. Tip area function was calibrated using fused quartz calibration standard prior to all measurements.

2.5. SEM analyses

SEM analyses were performed on Tescan Mira GMU electron microscope equipped with EDS detector (Oxford Instruments). Surface imaging was performed using SE and BSE imaging mode. EDS chemical mapping were performed over nanoindentation measurement areas for further identification of individual cement paste phases based on chemical composition.

2.6. Results and discussion

The elemental composition of the scanned cement paste area of the neutron irradiated concrete is shown as EDS sum spectrum and individual maps of the major elements in Figure 4. Majority of the area is composed of Ca-Si hydrate phase (C-S-H). Areas with dominant Ca concentration indicate the presence of portlandite $Ca(OH)_2$ phase. The Al map revealed the presence of larger patches of unreacted porous fly ash particles which are usually round or oval in shape. Residual clinker also occurs locally.

Identified phases are labelled in Figure 5a, which is a composition of selected EDS maps with SE image of the measured area on the background. The same image is complemented with SPM image with indent positions overlay in Figure 5b.

Despite the visible scratches caused by dry hand grinding preparation method, the resulting microstructure visibility, and surface flatness of the cement paste area of the concrete were sufficient for precise indent

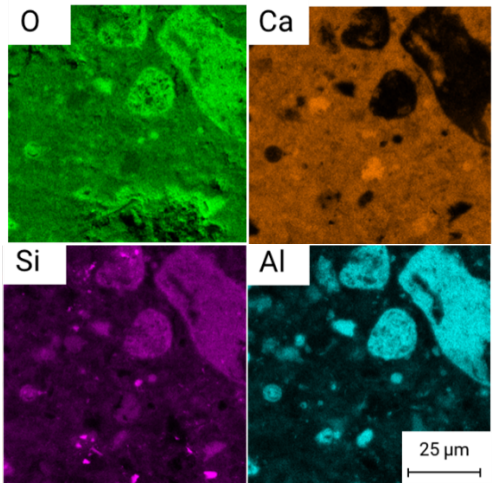

Figure 4. Distribution of selected elements in the cement paste of neutron irradiated concrete analysed by SEM EDS.

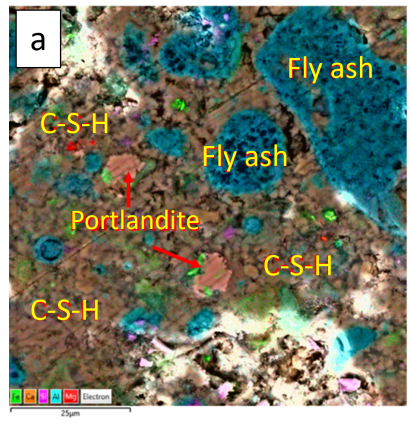

(a).

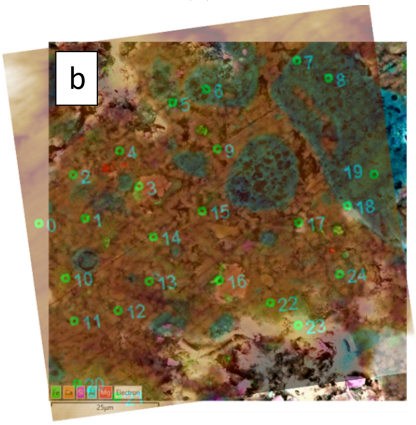

(b).

Figure 5. Selected elemental distribution maps overlay on SE image of indented area (a) and the same image combined with SPM image with highlighted indent positions (b).

positioning in the SPM nanoindentation mode. Measured nanoindentation hardness (H_{it}) and reduced modulus (Er) results relative to the identified phases are shown in Figure 6a, 6b. The difference between each phase is clearly visible for both H_{it} and Er val-

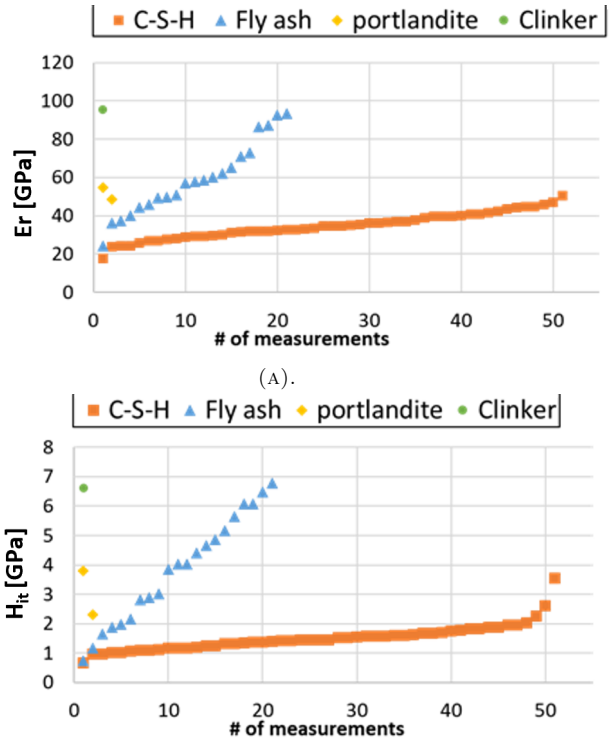

FIGURE 6. Comparison of measured reduced modulus (Er) and hardness (H_{it}) between identified phases in cement paste area of the neutron irradiated concrete.

ues. However, without phase identification knowledge gained with the use of correlation of SEM-EDS and SPM scans, lower measured values of fly ash and portlandite would be easily mixed with C-S-H gel values. The same applies for high fly ash values and clinker.

The high scatter of measured nanoindentation values for fly ash is most likely caused by high porosity of the particles. This causes variations in indenter tip contact and uneven deformation area during nanoindentation testing. The variance of measured values of the C-S-H phase is likely caused by multiple factors. First, the surface in the C-S-H area is uneven and to certain extent porous, which means that same nanoindentation effects as for the fly ash phase will apply for C-S-H phase. And second, from previous investigation it is known that C-S-H phase can be divided into two sub-categories: low density (LD) and high density (HD) C-S-H [11]. These two types of C-S-H vary in mechanical properties, thus create the variety of measured results. The C-S-H phases present in cement paste are mixed with other minor phases and are specifically designated as inner (HD) and outer (LD) product [12]. Using SEM SE imaging on the reference concrete (Figure 7a, 7b), HD C-S-H areas are visible as lighter areas and LD C-S-H as darker. However, this differentiation is not possible on neutron irradiated concrete, as is shown in Figure 7, where both C-S-H products are not distinguishable. Therefore, it is to be assumed that it is a mixture of both LD and HD types.

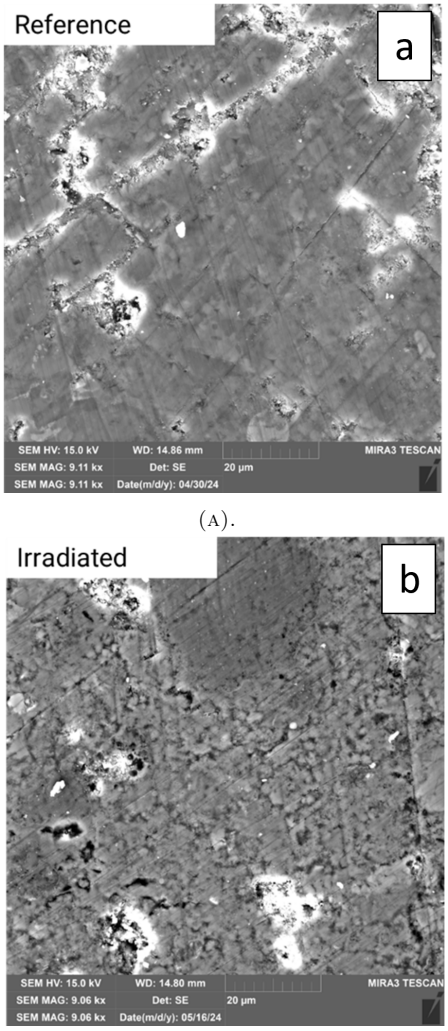

FIGURE 7. SE image of C-S-H gel distribution on reference non-irradiated concrete (a) and neutron irradiated concrete (b).

Although it was previously assumed that the effects of neutrons on cement paste would be small or negligible [13, 14], recent research suggests that degradation of cement paste components due to neutron interaction also needs to be considered. The change of surface morphology and chemical bonding of C-S-H globules after irradiation was reported by [15]. Other authors have described changes in nano-porosity due to the effects of radiolysis, carbonation [16], formation of secondary vaterite [16], and, on the other hand, also a certain self-healing effect in C-S-H gels [17].

A comparison of Er and H_{it} of LD and HD C-S-H phases from nanoindentation measurements on reference non-irradiated concrete and mixed C-S-H phase from nanoindentation measurements on neutron and gamma irradiated concrete was made. The results shown in Figure 8 indicate that the measured values of the irradiated C-S-H phase are in between the values of the HD and LD C-S-H on reference material and we observe a greater scatter in the measured Er and H_{it} values of the neutron-irradiated C-S-H phase. This

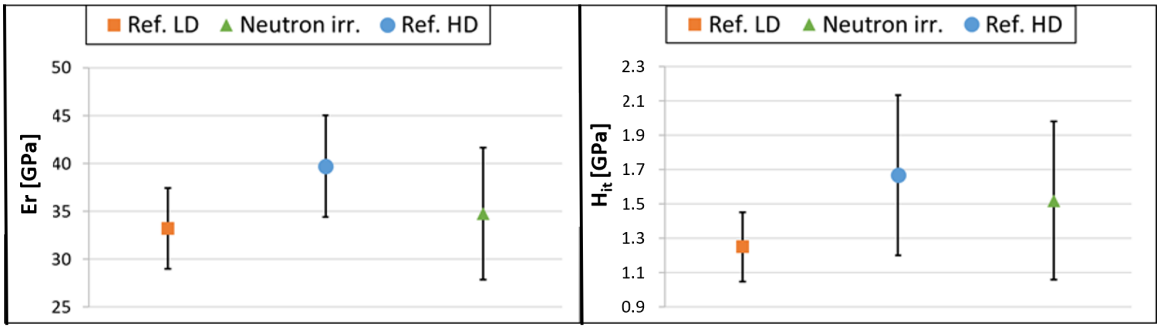

Figure 8. Comparison of averaged nanoindentation results of Er and H_{it} of low density (LD) and high density (HD) C-S-H phase on reference non-irradiated concrete and mixed C-S-H phase on neutron and gamma irradiated concrete.

measurement supports the previous findings that the neutron irradiation has an effect on the mechanical behavior of the C-S-H phase. This effect is to be verified by further investigation.

2.7. Conclusions

Nanomechanical properties of the hydrated cement phases after neutron irradiation were investigated and these conclusions can be drawn:

- It was verified that the dry grinding surface preparation method for nanoindentation measurements is suitable for neutron-irradiated concrete.
- SEM images in combination with SEM-EDS chemical maps over the indented cement areas provided useful identification of the measured phases. Measured mechanical properties were linked to the individual phases creating, separated datasets for each measured phase.
- The correlative approach effectively compares overlapping phase data, which is challenging with large array methods without phase identification, and combining both methods yields extensive statistical data with improved phase identification.
- The LD and HD types of the C-S-H phase in neutron-irradiated concrete appear indistinguishable in SEM images, indicating altered properties due to irradiation. The measured Er and H_{it} values of the neutron-irradiated C-S-H phase show greater variability compared to non-irradiated material.

List of symbols

NPP Nuclear Power Plant
VVER-440 Water-Water Power Reactor with electrical output of 440 MW
SEM Scanning Electron Microscope
EDS Energy-dispersive Spectroscopy
SPM Scanning Probe Microscopy
SE Secondary electron Image
BSE Backscattered Electron Image
PVD Physical Vapor Deposition
C-S-H Calcium-Silicate Hydrate
H_{it} Hardness [GPa]
Er Reduced Modulus [GPa]
LD Low Density C-S-H gel
HD High Density C-S-H gel

Acknowledgements

This work was financially supported by the project of the Czech Science Foundation grant number 23-05435S. The presented results were obtained using the CICRR infrastructure, which is financially supported by the Ministry of Education, Youth and Sports – project LM2023041.

References

[1] K. L. Murty, I. Charit. Structural materials for Gen-IV nuclear reactors: Challenges and opportunities. *Journal of Nuclear Materials* **383**(1):189–195, 2008. Advances in Nuclear Materials: Processing, Performance and Phenomena. https://doi.org/10.1016/j.jnucmat.2008.08.044

[2] L. Malerba, A. Al Mazouzi, M. Bertolus, et al. Materials for sustainable nuclear energy: A European strategic research and innovation agenda for all reactor generations. *Energies* **15**(5):1845, 2022. https://doi.org/10.3390/en15051845

[3] H. K. Hilsdorf, J. Kropp, H. J. Koch. The effects of nuclear radiation on the mechanical properties of concrete. *American Concrete Institute Symposium Publication* **55**:223–254, 1978. https://doi.org/10.14359/6616

[4] K. G. Field, I. Remec, Y. Le Pape. Radiation effects in concrete for nuclear power plants – Part i: Quantification of radiation exposure and radiation effects. *Nuclear Engineering and Design* **282**:126–143, 2015. https://doi.org/10.1016/j.nucengdes.2014.10.003

[5] W. R. L. da Silva, J. Němeček, P. Štemberk. Methodology for nanoindentation-assisted prediction of macroscale elastic properties of high performance cementitious composites. *Cement and Concrete Composites* **45**:57–68, 2014. https://doi.org/10.1016/j.cemconcomp.2013.09.013

[6] L. Sorelli, G. Constantinides, F.-J. Ulm, F. Toutlemonde. The nano-mechanical signature of Ultra High Performance Concrete by statistical nanoindentation techniques. *Cement and Concrete Research* **38**(12):1447–1456, 2008. https://doi.org/10.1016/j.cemconres.2008.09.002

[7] W. Zhu, J. J. Hughes, N. Bicanic, C. J. Pearce. Nanoindentation mapping of mechanical properties of cement paste and natural rocks. *Materials Characterization* **58**(11):1189–1198, 2007. 10th Euroseminar on Microscopy Applied to Building Materials (EMABM). https://doi.org/10.1016/j.matchar.2007.05.018

[8] V. Gorgol. Concrete – Part 1: Specification, performance, production and conformity, 2000. Czech Office for Standardization and Metrology Testing, Prague, Czech Republic, Standard No. ČSN EN 206-1.

[9] T. Melichar, Z. Hlaváč, J. Šoltés, et al. Vývoj a využití zařízení pro ozařování betonových vzorků v jaderném reaktoru LVR-15. *Jaderná Energie* **4**:38–43, 2022.

[10] W. C. Oliver, G. M. Pharr. An improved technique for determining hardness and elastic modulus using load and displacement sensing indentation experiments. *Journal of materials research* **7**(6):1564–1583, 1992. https://doi.org/10.1557/JMR.1992.1564

[11] G. Constantinides, F.-J. Ulm. The effect of two types of C-S-H on the elasticity of cement-based materials: Results from nanoindentation and micromechanical modeling. *Cement and Concrete Research* **34**(1):67–80, 2004. https://doi.org/10.1016/S0008-8846(03)00230-8

[12] Y. Yan, J. Tang, G. Geng. Exploring microstructure development of C-S-H gel in cement blends with starch-based polysaccharide additives. *Case Studies in Construction Materials* **19**:e02589, 2023. https://doi.org/10.1016/j.cscm.2023.e02589

[13] I. Maruyama, O. Kontani, M. Takizawa, et al. Development of soundness assessment procedure for concrete members affected by neutron and gamma-ray irradiation. *Journal of Advanced Concrete Technology* **15**(9):440–523, 2017. https://doi.org/10.3151/jact.15.440

[14] O. Kontani, Y. Ichikawa, A. Ishizawa, et al. Irradiation effects on concrete structures. In *Infrastructure Systems for Nuclear Energy*, pp. 459–473. 2014. https://doi.org/10.1002/9781118536254.ch27

[15] K. Park, C.-W. Chung, C. J. Lee, T.-H. Kwon. Investigation of irradiation effects on microstructure of cement paste using small-angle neutron scattering. *Cement and Concrete Research* **123**:105791, 2019. https://doi.org/10.1016/j.cemconres.2019.105791

[16] Y. Le Pape. 3.18 – radiation effects in concrete for nuclear systems. In R. J. M. Konings, R. E. Stoller (eds.), *Comprehensive Nuclear Materials (Second Edition)*, pp. 592–614. 2020. https://doi.org/10.1016/B978-0-12-803581-8.11617-0

[17] A. Alex, B. Freeman, A. Jefferson, E. Masoero. Carbonation and self-healing in concrete: Kinetic Monte Carlo simulations of mineralization. *Cement and Concrete Composites* **144**:105281, 2023. https://doi.org/10.1016/j.cemconcomp.2023.105281